Spin dynamics of an isotropic singlet-ground-state antiferromagnet with alternating strong and weak interactions: An inelastic-neutron-scattering study of the dimer compound $Cs_3Cr_2Br_9$

B. Leuenberger,* A. Stebler, and H. U. Güdel*
Institut für Anorganische Chemie, Universität Bern, CH-3000 Bern 9, Switzerland

A. Furrer
Laboratorium für Neutronenstreuung, ETHZ, CH-5303 Würenlingen, Switzerland

R. Feile† and J. K. Kjems
Risø National Laboratory, DK-4000 Roskilde, Denmark
(Received 18 May 1984)

Powder and single-crystal samples of the dimer compound $Cs_3Cr_2Br_9$ have been studied by inelastic neutron scattering. At 1.6 K, the singlet-to-triplet dimer excitation exhibits pronounced energy dispersion as a result of weak interdimer interactions. The results are interpreted within the random-phase approximation with use of a Heisenberg Hamiltonian and considering only nearest-neighbor interactions. The agreement between theory and experiment is excellent. Three exchange parameters have been obtained at 1.6 K: $J=-1.03$ meV (intradimer), $J_p=-0.054$ meV (interdimer, intrasublattice), and $J_c=-0.039$ meV (interdimer, intersublattice). The excitation shows soft-mode behavior. However, an ordering does not occur above 1.6 K.

INTRODUCTION

Clusters of exchange-coupled paramagnetic ions have attracted much scientific interest.[1] In most studies the compound under consideration contained well-isolated clusters, either by nature or by doping a host lattice with a small amount of paramagnetic ions. Therefore, intercluster interaction was rarely important and the experimental data could be well interpreted on the basis of molecular clusters. The presence of intercluster interactions provides a distinctly new situation. The simple molecular picture is no longer appropriate and the situation is characterized by alternating strong (intracluster) and weak (intercluster) interactions. Such alternating systems are of interest from an experimental and theoretical point of view[2] due to their different properties compared to systems containing only interactions of equal strength. $Cs_3Cr_2Br_9$ provides a particularly attractive example of an alternating system. The strong antiferromagnetic exchange within the $Cr_2Br_9^{3-}$ dimers produces an isotropic singlet ground state. At low temperature, therefore, there is a competition between the intradimer and interdimer interactions, driving the system towards diamagnetic and antiferromagnetic behavior, respectively. Much effort has been devoted to the question of under what conditions singlet-ground-state systems can order magnetically.[3] The singlet ground states of the rare-earth and transition-metal ions studied so far result from spin-orbit and anisotropic crystal-field interactions. As such they have to be considered as pseudosinglet states. In $Cs_3Cr_2Br_9$ the physical situation is completely different. The singlet-triplet splitting is the result of an isotropic intradimer exchange interaction. Interdimer exchange is only important between nearest neighbors, in contrast to most of the rare-earth systems, which are metallic with RKKY type of exchange.[3] $Cs_3Cr_2Br_9$ thus emerges as a system which lacks many of the complications of other singlet-ground-state magnets. $Cs_3Cr_2Br_9$ belongs to a large family of compounds $A_3M_2X_9$ ($A=Rb^+,Cs^+$; $M=Ti^{3+},V^{3+},Cr^{3+},Fe^{3+},Mo^{3+}$; $X=Cl^-,Br^-,I^-$) crystallizing in the hexagonal space group $P6_3/mmc$.[4] The structure is shown in Fig. 1. There are two $Cr_2Br_9^{3-}$ dimers per unit cell, both oriented along the hexagonal c axis, and we consider them to form two sublattices. The Cr-Cr separation is 3.3 Å within the dimers and 7.4 Å (intrasublattice) and 7.5 Å (intersublattice) between nearest-neighbor dimers. There are Cr-Br $\cdots$ Br-Cr contacts between the dimers, which provide pathways for weak interdimer interaction.

The low-temperature magnetic and spectroscopic properties of $Cs_3Cr_2Br_9$ and the related $Cs_3Cr_2Cl_9$ have so far been interpreted in purely molecular models, i.e., as resulting from the antiferromagnetic intradimer exchange[5]

$$\mathcal{H}=-J\vec{S}_1\cdot\vec{S}_2 \ . \tag{1}$$

Singlet-triplet separations were estimated to lie between 0.6 and 1.7 meV for the two compounds.[5] EPR spectra of $Cs_3Cr_2Cl_9$ at higher temperatures, where the triplet dimer level becomes populated, showed some evidence of interdimer exchange.[6]

In a brief communication[7] we have recently demonstrated the collective nature of the magnetic excitations of $Cs_3Cr_2Br_9$ at 1.6 K by inelastic neutron scattering (INS). This technique is one of the most powerful in the study of the interplay of alternating strong and weak interactions. In the present paper we give a detailed account of our experimental and theoretical work on $Cs_3Cr_2Br_9$.

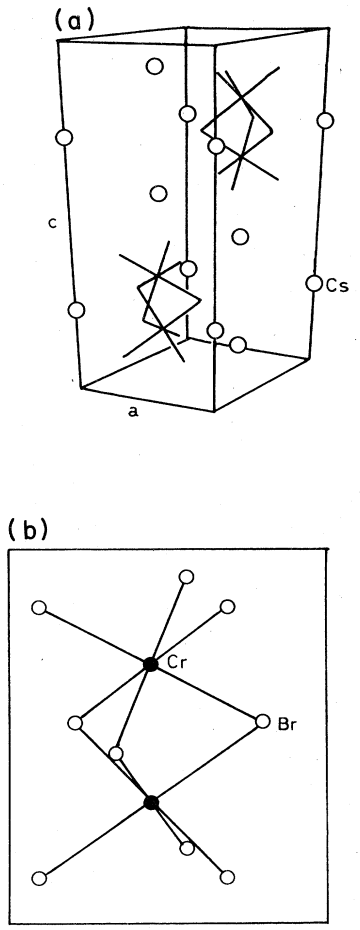

FIG. 1. (a) Hexagonal unit cell of $Cs_3Cr_2Br_9$. The two $Cr_2Br_9^{3-}$ units form the two sublattices. The lattice constants are $a=7.507$ Å and $c=18.68$ Å at room temperature. (b) $Cr_2Br_9^{3-}$ dimer. The point-group symmetry is D_{3h} and the Cr-Cr separation 3.3 Å.

EXPERIMENTAL

$Cs_3Cr_2Br_9$ was prepared from stoichiometric mixtures of CsBr and $CrBr_3$ in quartz tubes at 800 °C. A single crystal of about 2 cm^3 was grown from the mixture of CsBr and $CrBr_3$ by using the Bridgman technique. The quartz tube was charged with a thin film of graphite in order to prevent the building of a network between the tube and the crystal. The crystals are very fragile, soft, and air sensitive.

For the neutron-scattering experiments crystals and powder samples were mounted in aluminum cans under helium gas. All manipulations were performed in a glove box under dry nitrogen or helium.

The powder samples were checked by x-ray and neutron diffraction. The crystal was checked and oriented on a two-axis neutron spectrometer. The final orientation of the crystal was done with a four-circle neutron diffractometer. The mosaic of the crystal was 1°.

INS experiments on powder samples were carried out both at the reactor SAPHIR, Würenlingen, and at the reactor DR3, Risø, using triple-axis spectrometers. Extensive INS experiments were performed with the single crystal mounted in a pumped He cryostat on the triple-axis spectrometer TAS7, which is located at the cold source of the reactor DR3 at Risø. The final energy was fixed to 5 meV in these experiments and the beam collimation was typically 60'-40'-40'-40'. In order to remove higher-order contamination a cooled Be filter was placed in front of the analyzer.

THEORY

Cr^{3+} has an orbital singlet ground state $^4A_2$ in octahedral coordination. The single-ion anisotropy is small[6] and we can interpret all the experimental results reported here neglecting anisotropy terms. The Heisenberg Hamiltonian (1) provides an adequate description of the intradimer exchange. The resulting energies of the dimer follow a Landé splitting pattern, as shown in Fig. 2. Including interdimer exchange the following isotropic Hamiltonian is adequate for $Cs_3Cr_2Br_9$:

$$\mathcal{H}=-\tfrac{1}{2}\sum_{i,j,\mu,\nu} J_{i\mu j\nu}\vec{S}_{i\mu}\cdot\vec{S}_{j\nu}\,, \tag{2}$$

where i,j designate dimers and μ,ν the Cr^{3+} ions on the dimers i and j, respectively. The sum in Eq. (2) includes first- and second-shell neighbors of a given Cr^{3+} ion. There is only one neighbor in the first shell corresponding to the intradimer term $J=J_{i\mu i\nu}$. In the second shell there are six Cr^{3+} ions on neighboring dimers of the same sublattice ($J_p=J_{i\mu j\mu}$) and three Cr^{3+} ions on dimers of the other sublattice ($J_c=J_{i\mu j'\nu}$). The three parameters defining our system are shown in the schematic of Fig. 3.

Due to the different interaction strengths the intradimer exchange needs to be treated exactly. We define

$$\vec{K}_i=\vec{S}_{i1}+\vec{S}_{i2},\quad \vec{L}_i=\vec{S}_{i1}-\vec{S}_{i2}\,. \tag{3}$$

$\vec{K}_i$ is the dimer spin operator and $\vec{L}_i$ we will call pseudo-dimer spin operator. Using Eq. (3) the Hamiltonian (2)

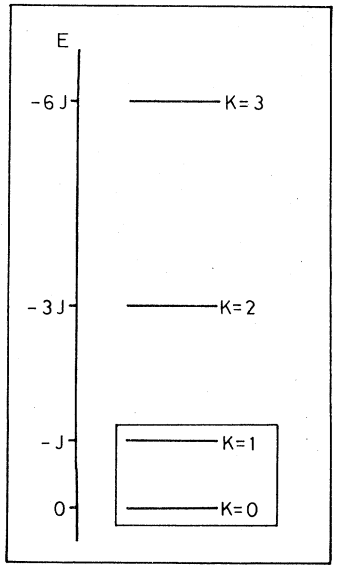

FIG. 2. Exchange splitting of the $Cr_2Br_9^{3-}$ dimer according to Hamiltonian (1).

can be written as

$$\mathcal{H}=\mathcal{H}_0+\mathcal{H}_K+\mathcal{H}_L ,$$

where

$$\mathcal{H}_0=-\frac{1}{4}J\sum_i(\vec{\mathrm{K}}_i\cdot\vec{\mathrm{K}}_i-\vec{\mathrm{L}}_i\cdot\vec{\mathrm{L}}_i) ,$$

$$\mathcal{H}_K=-\frac{1}{4}\left[J_p\sum_{i,j}\vec{\mathrm{K}}_i\cdot\vec{\mathrm{K}}_j+J_c\sum_{i,j'}\vec{\mathrm{K}}_i\cdot\vec{\mathrm{K}}_{j'}\right] , \tag{4}$$

$$\mathcal{H}_L=-\frac{1}{4}\left[J_p\sum_{i,j}\vec{\mathrm{L}}_i\cdot\vec{\mathrm{L}}_j-J_c\sum_{i,j'}\vec{\mathrm{L}}_i\cdot\vec{\mathrm{L}}_{j'}\right] .$$

$\mathcal{H}_0$ is the dimer Hamiltonian producing the Landé splitting pattern in Fig. 2. Since we are mainly interested in the singlet-triplet dimer excitations at temperatures below 10 K we neglect, in the following, the quintet and septet dimer levels lying at energies of approximately 3 and 6 meV, respectively.

$\mathcal{H}_K$ has the form of a normal Heisenberg Hamiltonian, but the interacting spins are dimer spins rather than single-ion spins. $\mathcal{H}_L$ represents the interaction between the pseudodimer spins. It is interesting to note that the intersublattice term of $\mathcal{H}_L$ has a positive sign. Its manifestation will therefore appear to be ferromagnetic for an antiferromagnetic interaction. $\vec{\mathrm{K}}$ is diagonal in the singlet-triplet dimer spin space, whereas $\vec{\mathrm{L}}$ is completely off-diagonal. It is therefore the term $\mathcal{H}_L$ which produces the dispersion of the singlet-triplet excitation, and $\mathcal{H}_K$ is neglected for this calculation.

In order to use the random-phase approximation (RPA) to decouple the equation of motion, we start by writing our Hamiltonian in terms of the so-called standard basis operators (SBO):[8]

$$\mathcal{H}=\sum_{i,n}E_n a^i_{nn}-\frac{1}{4}\left[J_p\sum_{i,j,m,n,m',n'}a^i_{mn}a^j_{m'n'}S_{mnm'n'}-J_c\sum_{i,j',m,n,m',n'}a^i_{mn}a^{j'}_{m'n'}S_{mnm'n'}\right] , \tag{5}$$

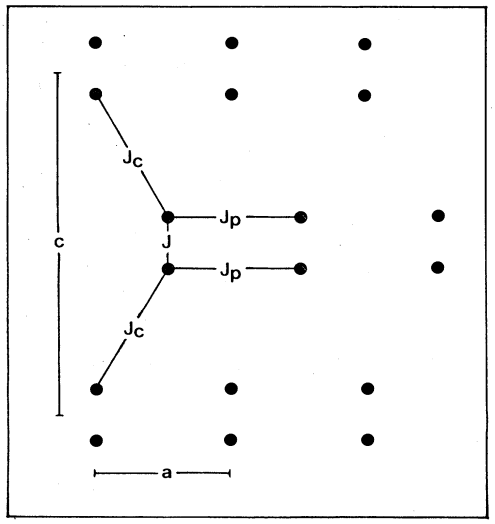

FIG. 3. Schematic structure of $Cs_3Cr_2Br_9$. The three interactions J (intradimer), J_p (interdimer, intrasublattice), and J_c (interdimer, intersublattice) are indicated.

where m,n and m',n' number the dimer states. E_n is the energy of the dimer state n, with E_0 defined as $E_0=0$ and, consequently, $E_1=-J$. a^i_{mn} is an SBO of dimer i, defined as

$$a^i_{mn}=(\,|\,m\,\rangle\langle\,n\,|\,)_i . \tag{6}$$

$S_{mnm'n'}$ contains matrix elements of $\vec{\mathrm{L}}$ as follows:

$$S_{mnm'n'}=\sum_\alpha\langle m\,|\,L^\alpha\,|\,n\rangle\langle m'\,|\,L^\alpha\,|\,n'\rangle . \tag{7}$$

The sum is over the Cartesian components α. Two sets of time- and temperature-dependent Green's functions are defined

$$G^{ij}_{mnm'n'}(t)=\langle\langle a^i_{mn}(t),a^j_{m'n'}(0)\rangle\rangle ,$$
$$G^{ij'}_{mnm'n'}(t)=\langle\langle a^i_{mn}(t),a^{j'}_{m'n'}(0)\rangle\rangle , \tag{8}$$

where the double angular brackets are defined by Zubarev.[9] The RPA is used to decouple the equation of motion of the Green's functions (8). After Fourier transformation in space and time we obtain

$$G^{\text{acoustic/optic}}_{prp'r'}(\vec{\mathrm{q}},\omega)(E_r-E_p-\omega)-\tfrac{1}{2}\sum_{m,n}[J_p\gamma_p(\vec{\mathrm{q}})\mp J_c\,|\,\gamma_c(\vec{\mathrm{q}})\,|\,]S_{mnrp}(n_p-n_r)G^{\text{acoustic/optic}}_{mnp'r'}(\vec{\mathrm{q}},\omega)=-\frac{1}{2\pi}(n_p-n_r)\delta_{pr'}\delta_{p'r} . \tag{9}$$

n_p is the population factor of the dimer state $|\,p\,\rangle$. $\gamma_p(\vec{\mathrm{q}})$ and $\gamma_c(\vec{\mathrm{q}})$ are the Fourier sums corresponding to the interactions J_p and J_c, respectively. They are given as follows:

$$\gamma_p(\vec{\mathrm{q}})=2[\cos(2\pi q_2)+\cos(2\pi q_1+2\pi q_2)+\cos(2\pi q_1)] ,$$
$$\gamma_c(\vec{\mathrm{q}})=2\cos(\pi q_3)\{\exp[i2\pi(q_1/3+2q_2/3)]+\exp[i2\pi(q_1/3-q_2/3)]+\exp[i2\pi(-2q_1/3-q_2/3)]\} . \tag{10}$$

$\gamma_c(\vec{\mathrm{q}})$ is complex and its phase is denoted by ϕ. The acoustic and optic Green's functions in (9) are defined as

$$G^{\text{acoustic/optic}}_{prp'r'}(\vec{\mathrm{q}},\omega)=G_{prp'r'}(\vec{\mathrm{q}},\omega)\pm e^{i\phi}G'_{prp'r'}(\vec{\mathrm{q}},\omega) , \tag{11}$$

where $G_{prp'r'}(\vec{\mathrm{q}},\omega)$ and $G'_{prp'r'}(\vec{\mathrm{q}},\omega)$ are the Fourier transforms of the Green's functions in (8). From (9) we obtain two triply degenerate singlet-triplet excitations:

$$\omega^{\text{acoustic/optic}}(\vec{q})=[J^2+M^2J(n_0-n_1)(J_p\gamma_p(\vec{q})\mp J_c\,|\,\gamma_c(\vec{q})\,|\,)]^{1/2}\ . \tag{12}$$

$M^2=5$ is the square of the singlet-to-triplet transition matrix element.

Comparing this result with the singlet-doublet system praseodymium, a representative example of the metallic rare-earth systems,[10] two interesting differences are observed. First, Eq. (12) contains only two interdimer exchange parameters, J_p and J_c, whereas in Pr many exchange parameters are needed due to the RKKY nature of the interaction. Second, in the dispersion relation for Pr the plus and minus signs in (12) are interchanged. The origin of this lies in the fact that in our dimer system the interaction producing the singlet-triplet dispersion is the interaction between pseudodimer spins rather than dimer spins. Physically this means that the interaction occurs between individual Cr^{3+} ions rather than Cr^{3+} dimers. Our next step is the evaluation of the inelastic neutron-scattering cross section for the magnetic excitations. It is given as[11]

$$\frac{d^2\sigma(\vec{\kappa},\omega)}{d\Omega\,d\omega}\sim F^2(\vec{\kappa})(1-e^{-\omega/kT})^{-1}\sum_{\alpha,\beta}\left[\delta_{\alpha\beta}-\frac{\kappa_\alpha\kappa_\beta}{\kappa^2}\right]\mathrm{Im}\bar{\chi}^{\alpha\beta}(\vec{\kappa},\omega)\ . \tag{13}$$

$\vec{\kappa}$ is the scattering vector $\vec{\kappa}=\vec{q}+\vec{\tau}$, where $\vec{\tau}$ is a reciprocal-lattice vector, $F(\vec{\kappa})$ is the form factor of Cr^{3+}, and $\bar{\chi}(\vec{\kappa},\omega)$ is the generalized susceptibility:

$$\bar{\chi}^{\alpha\beta}(\vec{\kappa},\omega)=i\int dt\sum_{j,d,e,\mu,\nu}e^{i\vec{\kappa}\cdot(\vec{r}_i+\vec{r}_d+\vec{r}_\mu-\vec{r}_j-\vec{r}_e-\vec{r}_\nu)}e^{i\omega t}\Theta(t)\langle[S^\alpha_{i+d+\mu},S^\beta_{j+e+\nu}]\rangle\ , \tag{14}$$

$\vec{r}_i,\vec{r}_j$ are the position vectors of the unit cells, $\vec{r}_d,\vec{r}_e$ denote the positions of the dimers in the unit cells i and j, and $\vec{r}_\mu,\vec{r}_\nu$ are the position vectors of the Cr^{3+} ions within the dimers d and e. $\Theta(t)$ is the step function. The susceptibility can be broken down as follows:

$$\bar{\chi}^{\alpha\beta}(\vec{\kappa},\omega)=2\chi^{\alpha\beta}(\vec{\kappa},\omega)+\chi'^{\alpha\beta}(\vec{\kappa},\omega)+\chi'^{\alpha\beta}(-\vec{\kappa},\omega)\ . \tag{15}$$

$\chi(\vec{\kappa},\omega)$ and $\chi'(\vec{\kappa},\omega)$ are the susceptibilities within and between the sublattices, respectively. By using the relation $\vec{\kappa}=\vec{q}+\vec{\tau}$ we obtain

$$\chi^{\alpha\beta}(\vec{\kappa},\omega)=\chi^{\alpha\beta}(\vec{q},\omega),\quad \chi'^{\alpha\beta}(\vec{\kappa},\omega)=\chi'^{\alpha\beta}(\vec{q},\omega)e^{i\vec{\rho}\,\vec{\tau}}\ , \tag{16}$$

where $\vec{\rho}$ is a vector connecting the two sublattices. In analogy to Eq. (8) the acoustic and optic susceptibilities are defined as

$$\chi^{\alpha\beta\ \text{acoustic/optic}}(\vec{q},\omega)=\chi^{\alpha\beta}(\vec{q},\omega)\pm e^{i\phi}\chi'^{\alpha\beta}(\vec{q},\omega)\ . \tag{17}$$

Using Eqs. (3) and (6) the spin operators in Eq. (14) are replaced by SBO and the Fourier transformation is executed. The susceptibility is then broken down as described above. By use of Eq. (9) we finally obtain

$$\chi^{\alpha\beta\ \text{acoustic/optic}}(\vec{q},\omega)=\chi_0^{\alpha\beta}(\omega)+\frac{J_p\gamma_p(\vec{q})\mp J_c\,|\,\gamma_c(\vec{q})\,|}{1-\cos(\vec{\kappa}\vec{R})}\sum_\gamma\chi_0^{\alpha\gamma}(\omega)\chi^{\gamma\beta\ \text{acoustic/optic}}(\vec{q},\omega)\ . \tag{18}$$

$\vec{R}$ is the vector connecting the two Cr^{3+} ions of a dimer, and $\chi_0(\omega)$ is the single dimer susceptibility

$$\chi_0(\omega)=-\tfrac{5}{2}[1-\cos(\vec{\kappa}\cdot\vec{R})](n_0-n_1)\left[\frac{1}{J-\omega}+\frac{1}{J+\omega}\right]\delta_{\alpha\beta}\ . \tag{19}$$

The interesting factor in Eqs. (18) and (19) is $[1-\cos(\vec{\kappa}\cdot\vec{R})]$. It does not appear in the corresponding expression for Pr.[10]

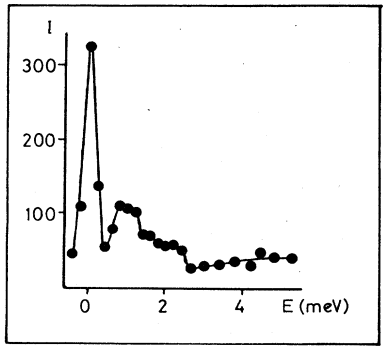

FIG. 4. Inelastic neutron scattering from a powder sample of $Cs_3Cr_2Br_9$ at 7 K and $\kappa=0.88$ Å^{-1}. The solid line is a guide for the eye.

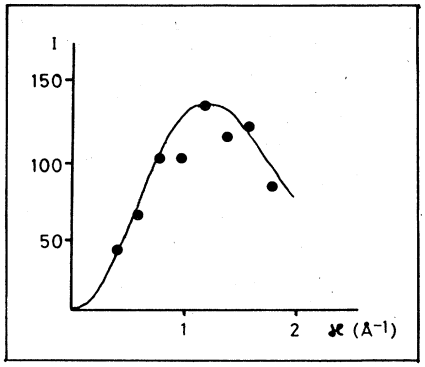

FIG. 5. Intensity of the singlet-triplet excitation as a function of κ in the powder sample of $Cs_3Cr_2Br_9$. The solid line represents the product $F^2(\vec{\kappa})\cdot[1+\sin(\vec{\kappa}\cdot\vec{R})/\kappa R]$ (Ref. 12).

This term produces the $\vec{\kappa}$ dependence of $\chi_0(\omega)$ and, therefore, of $\chi(\vec{q},\omega)$. It is an interference term which typically occurs in the INS cross section of dimer systems.[12] Combining Eqs. (13)—(19) we finally obtain for the cross section

$$\frac{d^2\sigma(\vec{\kappa},\omega)}{d\Omega\, d\omega} \sim F^2(\vec{\kappa})(1-e^{-\omega/kT})^{-1}(n_0-n_1)(-J)[1-\cos(\vec{\kappa}\cdot\vec{R})] \times \left[[1+\cos(\vec{\rho}\vec{\tau}+\phi)]\frac{1}{\omega^{\text{acoustic}}(\vec{q})}\delta(\omega-\omega^{\text{acoustic}}(\vec{q}))+[1-\cos(\vec{\rho}\vec{\tau}+\phi)]\frac{1}{\omega^{\text{optic}}(\vec{q})}\delta(\omega-\omega^{\text{optic}}(\vec{q}))\right] . \quad (20)$$

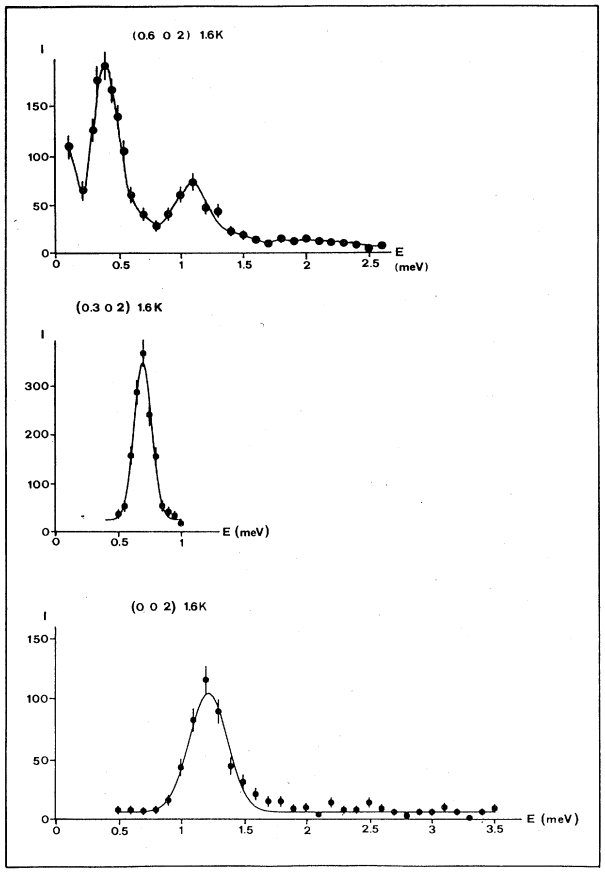

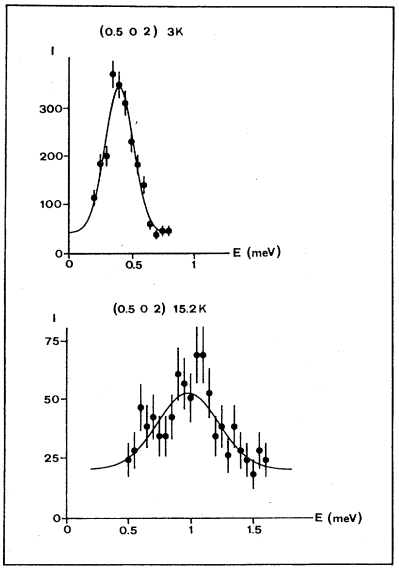

FIG. 6. Selected single-crystal INS scans illustrating the energy dispersion of the well-defined magnetic excitations.

RESULTS AND DISCUSSION

Figure 4 shows a powder INS spectrum of $Cs_3Cr_2Br_9$ at 7 K. It consists of two broad and poorly resolved features at energy transfers of approximately 1 and 2 meV. Figure 5 shows the intensity-versus-κ behavior of the 1-meV excitation. Its magnetic nature is evident from the dependence of the intensity on κ and the temperature. The 2-meV feature disappears on cooling to 1.6 K. We therefore assign the 1- and 2-meV features to singlet-triplet and triplet-quintet dimer excitations, respectively. In contrast to other Cr^{3+} dimer systems which have been investigated by INS (Ref. 13) the observed bands are broad. They must be broadened by a physical effect, because the instrumental resolution in Fig. 4 is better than 0.5 meV.

On the basis of these preliminary measurements we decided to investigate the singlet-triplet excitation in detail on a single crystal at low temperatures. Figure 6 shows a number of selected INS scans at 1.6 K. Obviously the excitation energy depends on the scattering vector, and this immediately explains the unusual width of the bands in the powder spectrum. At the (0.6,0,2) point in the Brillouin zone two excitations are observed in the INS spectrum. Systematic scans were taken in the symmetry directions of the crystal: Γ—A [001], Γ—K [110], and Γ—M [100]. Figure 7 shows the results of all the dispersion measurements at 1.6 K. Included in Fig. 7 is the result of a least-squares fit of the theoretical dispersion relation (12) to the data. The fit is excellent and the following parameter values were obtained:

$$\begin{aligned} J &= -1.03(1) \text{ meV} , \\ J_p &= -0.054(1) \text{ meV} , \\ J_c &= -0.039(1) \text{ meV} . \end{aligned} \quad (21)$$

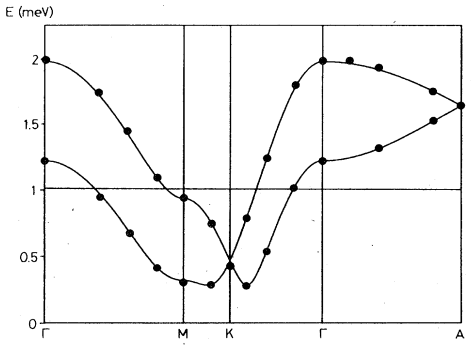

FIG. 7. Observed and calculated [Eq. (12)] excitation energies for the three symmetry directions of the hexagonal lattice: Γ—A (001), Γ—K (110), Γ—M (100). The parameters (21) were used for the calculation. The upper and lower branches correspond to the optic and acoustic modes, respectively. The horizontal line at 1.03 meV corresponds to $-J$.

(The values of J_p and J_c here are twice those reported in Ref. 7, because in the present paper the corresponding terms in the Hamiltonian are not multiplied by a factor of 2 for reasons of consistency with the parameter J.) Both J_p and J_c are antiferromagnetic. The acoustic and optic modes were distinguished on the basis of the factor $[1\pm\cos(\vec{\rho}\vec{\tau}+\phi)]$ in the scattering law (20). Figure 8 shows a comparison of observed and calculated energies and intensities in the three symmetry directions at 1.6 K. It shows that the parameters derived from the energy dispersion reproduce the relative intensities with remarkable accuracy, thus providing additional support for our theoretical model.

The antiferromagnetic sign and the similar magnitude of J_p and J_c are not unexpected. As the detailed structure shows, similar superexchange pathways Cr-Br · · · Br-Cr exist in both cases.

A contour plot of the acoustic mode in the basal plane, calculated using Eq. (12), is shown in Fig. 9. There is a flat ringlike trough around the K point with no preference

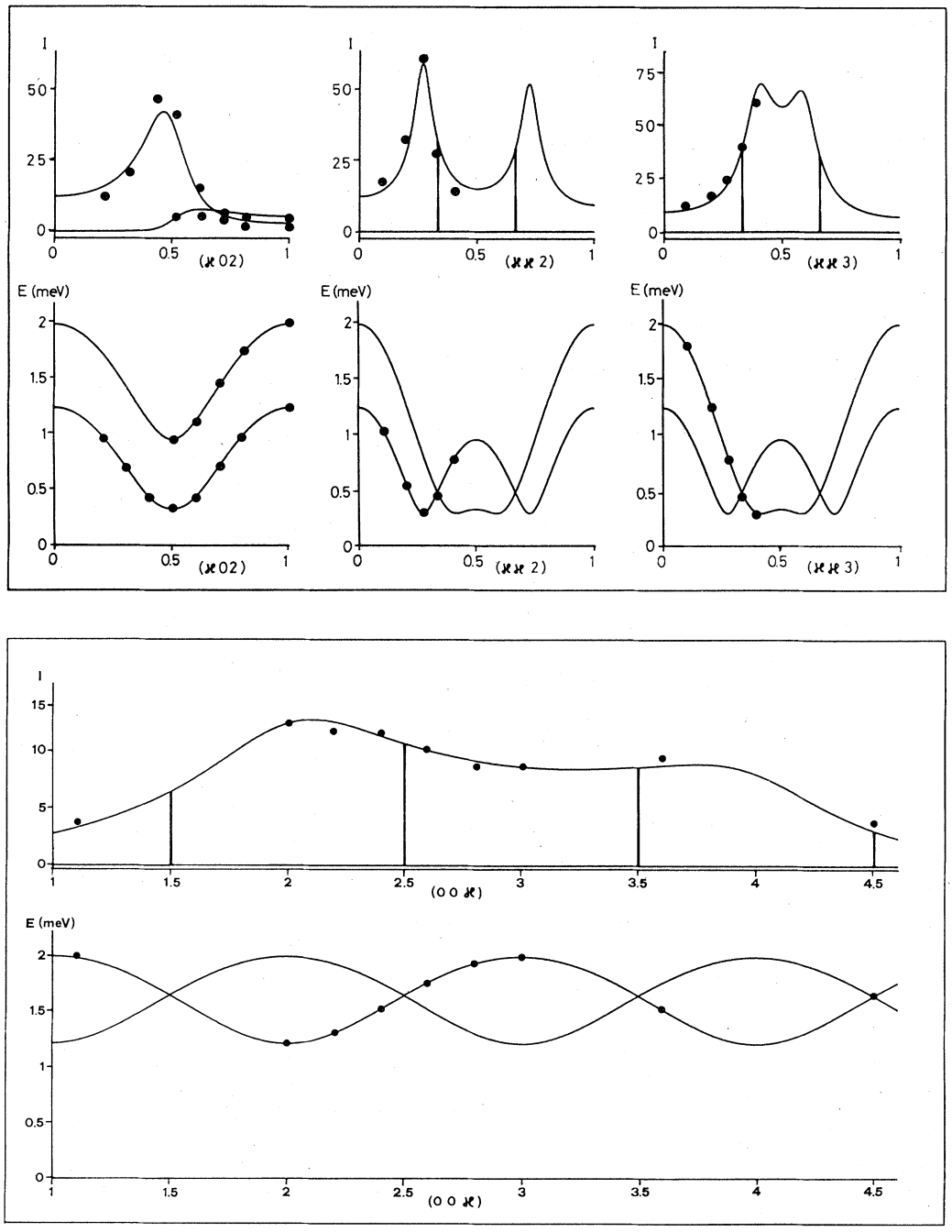

FIG. 8. Observed and calculated INS energies and intensities for the symmetry directions of the hexagonal lattice at 1.6 K. The calculation was performed by using Eqs. (12) and (20) and the parameters (21).

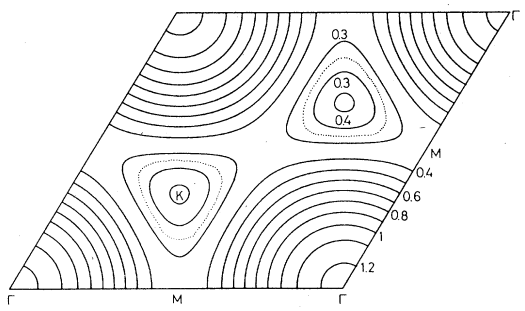

FIG. 9. Contour plot (in units of meV) of the acoustic mode at 1.6 K in the basal plane. The dotted line around the K point indicates the minimum.

for a potential ordering vector.

The temperature dependence of the acoustic mode was measured at the M point, which is close to the minimum energy of the dispersion. The results are plotted in Fig. 10. The observed behavior of both the energy and intensity of the excitation between 15 and 1.6 K is typical of a soft mode. At 1.6 K the softening is not complete, however, and on the basis of our theoretical model the system is not expected to order at lower temperature. The theoretical temperature dependences, derived using Eqs. (12) and (20), are included in Fig. 10. The excitation energy levels off below 1.5 K. Since the energy gap around the K point is below 0.3 meV at 1.6 K we cannot completely rule out the possibility that the system will order below 1.5 K due to some additional effects which have been neglected so far. Within our model we would expect the system to order if the ratio

$$|M^2J^*/J|\ , \qquad J^*=J_p\gamma_p(\vec{q}_0)-J_c\,|\gamma_c(\vec{q}_0)| \tag{22}$$

were larger than 1. With the exchange parameters (21) we obtain a value of 0.92 for this ratio and the system is therefore slightly undercritical.

The interdimer to intradimer exchange ratio (22) can be varied by physical and chemical perturbations. Since in $Cs_3Cr_2Br_9$ the ratio is very close to the required threshold for magnetic ordering, not too great a perturbation may be required to induce a phase transition to an ordered phase.

Application of an external magnetic field is the most straightforward physical perturbation. On the basis of Eq. (12) we estimate that at 1.6 K a field of $3T$ should be sufficient to induce magnetic order. We suspect, however, that anisotropy and correlation effects may become important as we approach the critical region. Chemical perturbations involve substitutions of Cs by Rb and Br by Cl or I. The latter are expected to be more important because they directly affect both the intradimer and interdimer exchange. For $Cs_3Cr_2Cl_9$ we expect an increase of J and a decrease of J^* resulting in a smaller ratio (22). Magnetic order is therefore not expected to occur at finite temperature. The trends are expected to be reversed for $Cs_3Cr_2I_9$, with J decreasing and J^* increasing, thus increasing the ratio (22) to above the threshold value. We are presently engaged in applying both physical and chemical perturbations to $Cs_3Cr_2Br_9$.

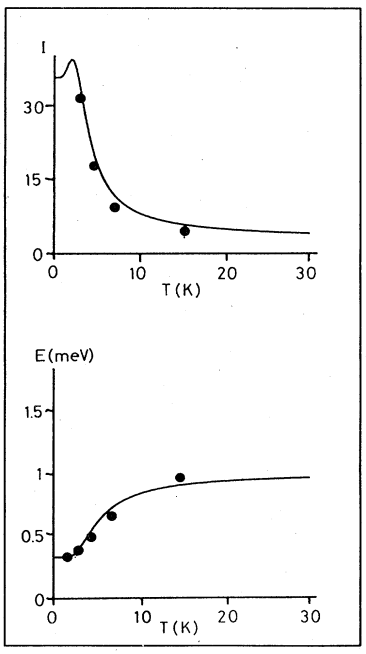

FIG. 10. Observed and calculated [by using Eqs. (12) and (20)] temperature dependence of the energy and intensity of the acoustic mode at the M point. The small decrease of the intensity towards the lowest temperatures may be an artifact of the RPA.

ACKNOWLEDGMENTS

Illuminating discussions with P. A. Lindgård and A. R. Mackintosh are acknowledged. This work was financially supported by the Swiss National Science Foundation. A travel grant by the Stiftung Zur Förderung der Wissenschaftlichen Forschung an der Universität Bern is gratefully acknowledged.

*To whom correspondence should be addressed.

†Present address: Institut für Physik, J. Gutenberg-Universität, D-6500 Mainz, Germany.

[1]Nato Asi, in *Magneto-Structural Correlations in Exchange-Coupled Systems*, edited by R. D. Willett (Reidel, Amsterdam, 1984).

[2]M. Tachiki and T. Yamada, Suppl. Prog. Theor. Phys. **46**, 291 (1970); N. Yamashita and K. Amaya, J. Phys. Soc. Jpn. **41**, 419 (1976); E. J. Samuelsen and M. Melamud, J. Phys. C **7**, 4314 (1974).

[3]P. Fulde, in *Handbook on the Physics and Chemistry of Rare Earths*, edited by A. Gschneidner and L. Eyring (North Hol-

land, Amsterdam, 1978); R. Birgeneau, in *Magnetism and Magnetic Materials—1972 (Denver),* proceedings of the 18th Annual Conference on Magnetism and Magnetic Materials, edited by C. D. Graham and J. J. Rhyne (AIP, New York, 1973).

[4]G. J. Wessel and D. J. W. Ijdo, Acta Crystallogr. **10**, 466 (1957); R. Saillant, R. B. Jackson, W. E. Streib, K. Folting, and R. A. D. Wentworth, Inorg. Chem. **10**, 1453 (1971).

[5]I. W. Johnstone, B. Briat, and D. Lockwood, Solid State Commun. **35**, 689 (1980); O. Kahn and B. Briat, Chem. Phys. Lett. **32**, 376 (1975); L. Dubicki, J. Ferguson, and B. V. Harrowfield, Mol. Phys. **34**, 1545 (1977); I. W. Johnstone, K. J. Maxwell, and K. W. H. Stevens, J. Phys. C **14**, 1297 (1981).

[6]J. R. Beswick and D. E. Dugdale, J. Phys. C **6**, 3326 (1973).

[7]B. Leuenberger, H. U. Güdel, R. Feile, and J. K. Kjems, Phys. Rev. B **28**, 5368 (1983).

[8]S. B. Haley and P. Erdös, Phys. Rev. B **5**, 1106 (1972).

[9]D. N. Zubarev, Usp. Fiz. Nauk **71**, 71 (1960) [Sov. Phys.—Usp **3**, 320 (1960)].

[10]P. A. Lindgård, J. Phys. C **8**, L178 (1975).

[11]W. Marshall and S. W. Lovesey, *Theory of Thermal Neutron Scattering* (Clarendon, Oxford, 1971), pp. 231 and 574.

[12]A. Furrer and H. U. Güdel, Phys. Rev. Lett. **39**, 657 (1977).

[13]H. U. Güdel, A. Furrer, W. Bührer, and B. Hälg, Surf. Sci. **106**, 432 (1981).